ISSN 1068-3356, Bulletin of the Lebedev Physics Institute, 2015, Vol. 42, No. 11, pp. 323–328. © Allerton Press, Inc., 2015.
Original Russian Text © I.A. Budagovsky, A.S. Zolot'ko, D.L. Korshunov, M.P. Smayev, S.A. Shvetsov, 2015, published in Kratkie Soobshcheniya po Fizike, 2015, Vol. 42, No. 11, pp. 24–32.

Optical Vortex Formation in the Field of the Gaussian Beam with High Degree of Wavefront Curvature when Passing Through Undeformed Nematic Liquid Crystal

I. A. Budagovsky[a], A. S. Zolot'ko[a], D. L. Korshunov[a,b], M. P. Smayev[a], and S. A. Shvetsov[a,b]

[a] *Lebedev Physical Institute, Russian Academy of Sciences, Leninskii pr. 53, Moscow, 119991 Russia; e-mail: smayev@lebedev.ru*
[b] *Moscow Institute of Physics and Technology, Institutskii per. 9, Dolgoprudnyi, Moscow oblast, 141700 Russia*
Received April 23, 2015

Abstract—Diffraction of the focused circularly polarized Gaussian beam passed through an undeformed homeotropic nematic liquid crystal is considered. The parameters of two coaxial Gaussian beams and two optical vortices formed behind the liquid-crystal layer are determined. The difference in the positions of foci of Gaussian beams and vortices appears in the experiment as interference ring patterns. The efficiency of the beam transformation to optical vortices is calculated.

DOI: 10.3103/S1068335615110044

Keywords: nematic liquid crystals, conoscopic pattern, singular beams, optical vortices.

Introduction. The high optical anisotropy of nematic liquid crystals (NLCs) causes their wide application to wavefront modulation as control birefringent elements. The possibility of changing the orientation of the NLC director (the unit vector that defines the preferred orientation of molecules and, hence, the optical axis direction) by a rather simple method (under external fields or by changing boundary conditions) makes it possible to develop optical devices forming the set wavefront singularities on their basis. Examples of such an element are q-plates proposed by Marrucci [1, 2]. When the q-plate is exposed to a circularly polarized light beam, wavefront singularities are formed in the region of the specially formed director distribution. The topological orientation defect with charge $q = 1$ setting the radially symmetric director distribution in the NLC layer plane is mostly used. Such a director field makes it possible to transform the Gaussian beam passing through the defect region to an optical vortex with moment (charge) $m = \pm 2$. Similar radially-symmetric deformation of the director can be obtained in NLCs, using the orienting light action [3, 4], additional external field [5], and Schlieren structures defects [6].

In uniaxial crystals, vortex beams can be formed in an optical scheme for observing the conoscopic pattern, i.e., when the necessary distribution of the optical axis rotation angle with respect to light beam rays is caused by the beam wavefront curvature [7–9]. In [10], it was theoretically shown that such approach allows the formation of singular beams with various focal planes. This was experimentally implemented by the example of $CaCO_3$ crystal 1 cm thick [11]. In liquid crystals, vortex beam formation was observed in [3] in a conoscopic optical scheme with sharp focusing; however, the possibility of obtaining a multifocal system was not considered.

In this study, we calculated the parameters of a converging circularly polarized light beam passed through a thin nematic liquid crystal layer (with a characteristic thickness of 10–100 μm). Depending on the curvature radius of the incident beam wavefront and crystal parameters, the optical vortex generation efficiency, positions of focal planes of beam components, and corresponding intensity distributions were determined. The system of two foci spaced by $\sim$10 μm when using NLCs 100 μm thick was experimentally observed.

Calculation of the converging beam diffraction in NLC. Let us consider a converging Gaussian beam normally incident on an NLC cell. The field at the crystal input is written as

$$E_G = A_0 e^{-u^2 + i\dfrac{u^2}{D_c}}, \tag{1}$$

where A_0 is the beam amplitude, $u = \dfrac{\rho}{w}$, ρ is the transverse coordinate in the crystal plane, w is the beam radius, $D_c = \dfrac{2R_c}{kw^2}$, k is the wavenumber, and R_c is the wavefront curvature radius.

All beam rays, except for the axial one, propagate at a certain nonzero angle θ to the NLC director; the extraordinary wave gains an additional phase shift. The refractive index for the extraordinary wave is given by

$$n_e \approx \sqrt{\varepsilon_\perp} + \delta n \sin^2\theta, \tag{2}$$

where $\delta n = \dfrac{(\varepsilon_\parallel - \varepsilon_\perp)\sqrt{\varepsilon_\perp}}{2\varepsilon_\parallel}$, $\varepsilon_\parallel$ and $\varepsilon_\perp$ are the permittivities for extraordinary and ordinary waves. At small angles $\theta \approx \dfrac{\rho}{R_c}$, the additional phase shift $S = kL\delta n \sin^2\theta$ can be written as

$$S(u) = \Psi_0 u^2 \nu^2, \tag{3}$$

where $\Psi_0 = kL\delta n K_r$, $\nu = \dfrac{w}{R_c}$, $K_r = \dfrac{2}{(n_e + n_o)}$ is the correction factor caused by beam refraction.

In the case of normal light incidence, the transition matrix in the basis of circular polarizations is given by

$$W = e^{iS_0(u) + \frac{iS(u)}{2}} \left\{ \cos\frac{S(u)}{2} \begin{pmatrix} 1 & 0 \\ 0 & 1 \end{pmatrix} + i \cdot \sin\frac{S(u)}{2} \begin{pmatrix} 0 & e^{-2i\varphi} \\ e^{2i\varphi} & 0 \end{pmatrix} \right\}, \tag{4}$$

where $S_0(u) = \dfrac{u^2}{D_c}$, φ is the polar coordinate. For the circular-polarized wave passed through the crystal, the expression for the field is written as

$$\mathbf{E} = E_G e^{iS_0(u) + \frac{iS(u)}{2}} \left\{ \cos\frac{S(u)}{2} \mathbf{e}_\pm + i \cdot \sin\frac{S(u)}{2} e^{\pm 2i\varphi} \mathbf{e}_\mp \right\}, \tag{5}$$

where $\mathbf{e}_\pm$ are the unit vectors of the circular polarization.

It follows from (5) that the light beam gains an additional component with wavefront phase twist (which causes a beam intensity minimum at the center) and opposite circular polarization. This component corresponds to the optical vortex with charge $m = \pm 2$, depending on the circular polarization handedness of the incident beam.

Substituting Eq. (5) into the Kirchhoff diffraction integral [12], we finally obtain

$$\mathbf{E}_{\text{diff}} = \frac{2A_0}{iD} e^{ikR^2/2z} \{ \mathbf{e}_\pm (C^{\text{focus}}_{\text{gauss}} + C^{\text{shift}}_{\text{gauss}}) - \mathbf{e}_\mp e^{\pm 2i\psi} (C^{\text{focus}}_{\text{vortex}} - C^{\text{shift}}_{\text{vortex}}) \}, \tag{6}$$

where

$$C^{\text{focus}}_{\text{gauss}} = \frac{1}{2\gamma_0} e^{-\tau^2/4\gamma_0}, \quad C^{\text{shift}}_{\text{gauss}} = \frac{1}{2\gamma} e^{-\tau^2/4\gamma},$$

$$C^{\text{focus}}_{\text{vortex}} = \frac{1}{2\gamma_0} e^{-\tau^2/8\gamma_0} \left[\frac{\operatorname{sh}\left(\frac{\tau^2}{8\gamma_0}\right)}{\frac{\tau^2}{8\gamma_0}} - e^{-\tau^2/8\gamma_0} \right],$$

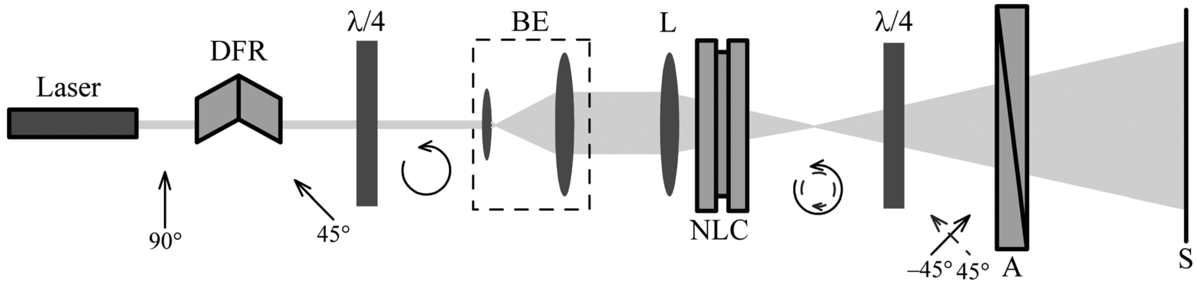

Fig. 1. Schematic of the experimental setup: DFR is the double Fresnel rhomb, $\lambda/4$ is the quarter-wave plate, BE is the beam expander, L is the lens, NLC is the cell with nematic liquid crystal, A is the analyzer, and S is the screen. Arrows indicate the radiation polarization direction, rotation angles of linear polarization are indicated with respect to the horizontal. Solid and dashed arrows correspond to Gaussian beam and optical vortex components, respectively.

$$C_{\rm vortex}^{\rm shift} = \frac{1}{2\gamma} e^{-\tau^2/8\gamma}\left[\frac{\operatorname{sh}\left(\frac{\tau^2}{8\gamma}\right)}{\frac{\tau^2}{8\gamma}} - e^{-\tau^2/8\gamma}\right],$$

$$D = \frac{2z}{kw^2},\ \tau = kw\theta,\ \gamma_0 = 1 - \frac{i}{D} - \frac{i}{D_c},\ \gamma = \gamma_0 - \frac{i}{D_{\rm NLC}},\ \frac{1}{D_{\rm NLC}} = \Psi_0\nu^2,$$

where R and ψ are the radial and polar coordinates in the observation plane.

Thus, the resulting expression is composed of four components corresponding to two optical vortices and two Gaussian beams with different parameters γ_0 and γ defining the wavefront curvature radius. For components $C_{\rm gauss}^{\rm shift}$ and $C_{\rm vortex}^{\rm shift}$, the waist position is shifted with respect to the focal plane of the Gaussian beam incident on NLC.

Results and discussion. Far from the focus, interference of components with different wavefront curvatures leads to patterns such as interference rings. These patterns were experimentally observed using a setup shown in Fig. 1. Linearly polarized radiation of the solid-state LASOS GL laser ($\lambda =$ 532 nm) passed through a double Fresnel rhomb allowing polarization plane rotation and a $\lambda/4$ plate (to obtain circular polarization). Then the beam was expanded and focused by a lens with focal length $f = 1$ cm, immediately behind which a cell with ZhKM-1277 NLC of homeotropic orientation was placed (the distance from the lens to the NLC layer was dictated by a cell glass substrate thickness equal to 1 mm). The beam radius on the lens was $w = 0.6$ cm. The ZhKM-1277 refractive indices for ordinary and extraordinary waves are $n_o = 1.52$ and $n_e = 1.71$. Vortical and Gaussian components were separated using one more $\lambda/4$ plate and the analyzer.

When NLC is exposed to linearly polarized light, the characteristic conoscopic pattern in crossed polarizers shaped as a dark cross (Fig. 2(a)) was observed on the screen; in parallel polarizers, the inverse pattern shaped as a bright cross was observed. When the crystal was exposed to circularly polarized light, components with different polarizations separately visualized at orthogonal analyzer positions $\xi = -45°$ (Fig. 2(b)) and $\xi = +45°$ (Fig. 2(c)) can be observed on the screen. A change in the power from 0.2 to 50 mW did not lead to a change in the pattern shape and sizes, which indicates the absence of appreciable orienting and thermal effects of light on NLC. The intermediate analyzer position $\xi = 0°$ allowed observation of interference of components (Fig. 2(d)).

Patterns 2(b) and 2(c) result from the interference of components with different focus positions. For example, the interference of Gaussian components with different wavefront curvatures results in the formation of the ring pattern with an intensity maximum at the center (Figs. 2(b) and 2(e)). The corresponding intensity profile is shown in Fig. 3 by solid curve. The interference of vortical components also leads to the formation of a ring pattern, but with an intensity minimum at the center (Figs. 2(c), 2(f) and Fig. 3, dashed curve). We note that summation of intensities of both patterns (in the experiment, this is achieved by analyzer removal) yields the Gaussian distribution (Fig. 3, dotted curve).

The conversion of the incident beam energy to the vortical beam energy depends on the beam tilt angle with respect to the director, i.e., is defined by w/R_c. At a sufficient focusing sharpness (which is necesssary for some problems of optical manipulation), the conversion value reaches 0.5 (Fig. 4).

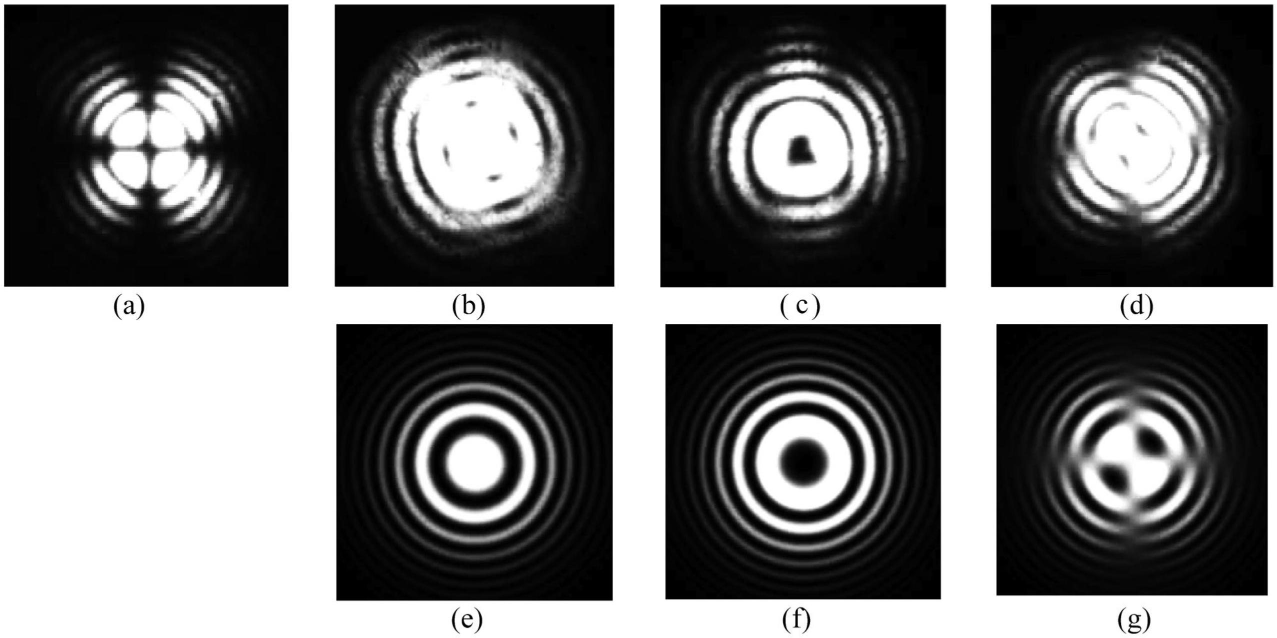

Fig. 2. Experimental ((a)–(d)) and calculated ((e)–(g)) intensity distributions of the light beam passed through the liquid-crystal layer, in the far-field region behind the analyzer. (a) Light beam intensity distribution in the far-field region in crossed polarizers. ((b), (e)) Diffraction of Gaussian radiation components (without vortex); ((c), (f)) diffraction of vortical components; ((d), (g)) interference of basic and vortical beam components ($\xi = 0°$). The angular size of frames is 0.8 rad. The light beam power in the experiment was 10 mW.

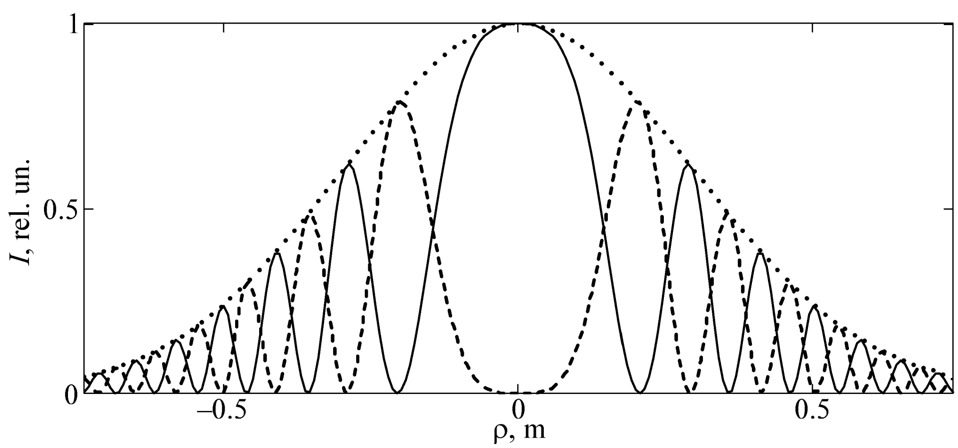

Fig. 3. Intensity profile far from focal planes ($z = 1$ m) for Gaussian (solid curve) and vortical (dashed curve) components and their sum (dotted curve) for the circularly polarized light beam passed through NLC.

Let us consider in more detail the features of the formation of components with different wavefront curvatures in the focal region ($z = 1$ cm). The positions of foci are spaced by the value defined by the parameter $D_{\rm NLC}$ which depends on the crystal thickness and optical anisotropy, $1/D_{\rm NLC} = kL\delta nK_r(w/R_c)^2$. The change in the wavefront curvature, introduced by the liquid crystal, can be considered as the effect of an additional lens with focal length $R_{\rm NLC} = \dfrac{kw^2}{2}D_{\rm NLC} = \dfrac{R_c^2}{2L\delta nK_r}$. Then the resulting curvature of the light wavefront can be determined from the relation $1/R_{\rm eff} = 1/R_c + 1/R_{\rm NLC}$. Since $R_c \ll R_{\rm NLC}$, then $R_{\rm eff} \approx R_c\left(1 - \dfrac{R_c}{R_{\rm NLC}}\right) = R_c - \Delta$, where $\Delta = 2L\delta nK_r$ is the distance be-

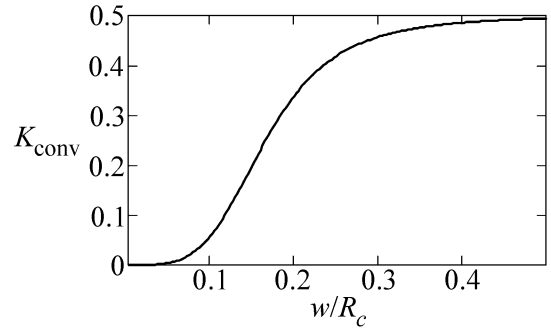

Fig. 4. Efficiency K_{conv} of the incident beam conversion to the vortical beam on the parameter w/R_c.

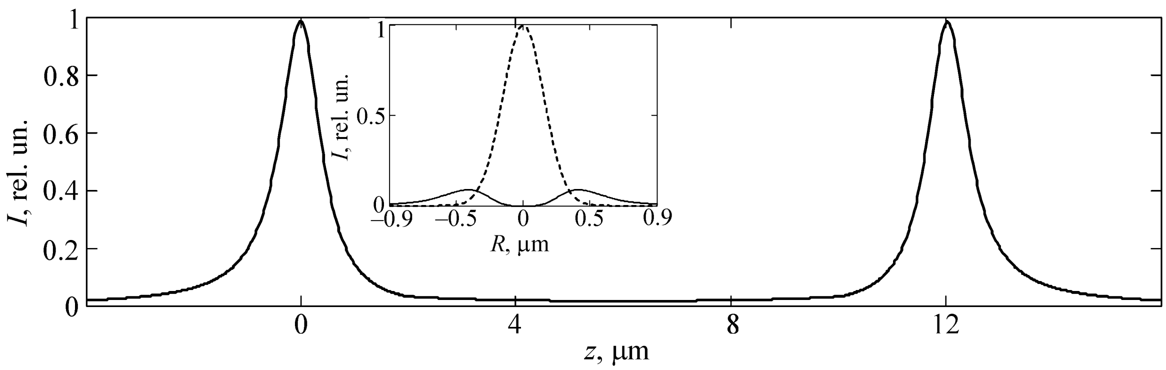

Fig. 5. Intensity distribution of Gaussian components on the beam axis near focal planes and the corresponding intensity profile in the cross section (inset) for vortical (solid curve) and Gaussian (dashed curve) components. The value $z = 0$ corresponds to the first focal plane position.

tween focal planes. The beam focusing by the lens before NLC almost does not affect Δ, since a change in the initial beam curvature radius controls not only the focus position, but also the beam tilt angle θ with respect to the NLC director. Changes in both parameters compensate each other. But the waist in focal planes, determined from the known expression $w_{\text{c,eff}}^2 = w^2\left(\left(1+\dfrac{z}{R_{\text{c,eff}}}\right)^2 + D^2\right)$ [12], will depend on initial focusing conditions.

The distance between interference rings makes it possible to estimate the distance Δ. The angular size θ_N of the ring with number N will be determined from the intensity maximum conditions during the interference of components with different wavefront curvatures,

$$\frac{k\Delta\theta_N^2}{2} = 2\pi N + \varphi_0, \tag{7}$$

where φ_0 is a constant; $0 \le \varphi_0 < 2\pi$. The calculation of Δ from experimental data by expression (7) yields $\Delta_e \sim 10 - 11$ μm which is consistent with theoretical $\Delta_r = 12$ μm.

A twofold decrease in the NLC thickness proportionally decreases Δ; in this case, the waist radius remains almost unchanged. Simultaneously, the waists, positions of foci, and the distance between them can be controlled using the lens placed behind the crystal.

The obtained expressions for positions of foci and beam sizes are valid for Gaussian components. The minimum transverse sizes of vortical components correspond to focal planes of Gaussian components (Fig. 5).

The power of the central ring of the vortical component in the present experiment is $P = 6$ mW at a laser radiation power of 50 mW. This value can be increased by selecting optimum NLC birefringence and focusing parameters. The bifocal system is attractive for problems of optical manipulation of microparticles, since it allows the development of a three-dimensional optical trap using a combination of two coaxial closely focused optical vortices. As experimentally shown in [13], such a system allows trapping and confinement of absorbing particles in air.

Conclusion. Propagation of the converging Gaussian beam through a thin layer of undeformed homeotropically oriented nematic liquid crystal was theoretically and experimentally studied. Analytical relations describing the formation of optical vortices were derived. It was shown that the light beam in the focus region is divided into two Gaussian and two vortical components with different wavefront curvature radii. For NLC 100 μm thick, the observed patterns correspond to generation of optical vortices and Gaussian beams with different focal planes spaced by $\sim$10 μm at the waist size of $\sim$1 μm.

ACKNOWLEDGMENTS

The authors are grateful to V. N. Ochkin for helpful discussions.

This study was supported by the Russian Science Foundation, project no. 14-12-00784.

REFERENCES

1. L. Marrucci, C. Manzo, and D. Paparo, Phys. Rev. Lett. **96**, 163905 (2006).
2. L. Marrucci, Mol. Cryst. Liq. Cryst. **488**, 148 (2008).
3. E. Brasselet, Opt. Lett. **34**, 3229 (2009).
4. E. Brasselet, Phys. Rev. A **82**, 063836 (2010).
5. R. Barboza, U. Bortolozzo, G. Assanto, et al., Phys. Rev. Lett. **109**, 143901 (2012).
6. C. Loussert, U. Delabre, and E. Brasselet, Phys. Rev. Lett. **111**, 037802 (2013).
7. A. V. Volyar and T. A. Fadeeva, Opt. Spektrosk. **94**, 264 (2003) [Opt. Spectrosc. **94**, 235 (2003)].
8. A. V. Volyar, Yu. A. Egorov, A. F. Rybas', and T. A. Fadeeva, Zh. Tekh. Fiz. **74**, 90 (2004) [Tech. Phys. **49**, 1627 (2004)].
9. A. V. Volyar, T. A. Fadeeva, and Yu. A. Egorov, Pisma Zh. Tekh. Fiz. Fiz. **28**, No. 22, 70 (2002) [Tech. Phys. Lett. **28**, 958 (2002)].
10. A. V. Volyar and T. A. Fadeeva, Opt. Spektrosk. **96**, 107 (2004) [Opt. Spectrosc. **96**, 96 (2004)].
11. V. G. Shvedov, C. Hnatovsky, N. Shostka, and W. Krolikowski, J. Opt. Soc. Am. B: Opt. Phys. **30**, 1 (2013).
12. M. B. Vinogradova, O. V. Rudenko, and A. P. Sukhorukov, *Theory of Waves* (Nauka, Moscow, 1979).
13. A. Turpin, V. Shvedov, C. Hnatovsky, et al., Opt. Express **21**, 26335 (2013).